arXiv:astro-ph/0211329v1 14 Nov 2002

The Neutrino Signal in Stellar Core Collapse and Postbounce Evolution

M. Liebendörfer[abc], A. Mezzacappa[b], O. E. B. Messer[ab], G. Martinez-Pinedo[de], W. R. Hix[ab], and F.-K. Thielemann[d]

[a]Department of Physics & Astronomy, University of Tennessee, Knoxville TN 37996

[b]Physics Division, Oak Ridge National Laboratory, Oak Ridge TN 37831

[c]Canadian Institute for Theoretical Astrophysics, Toronto ON M5S 3H8

[d]Department of Physics & Astronomy, University of Basel, Basel CH 4056

[e]Institut d'Estudis Espacials de Catalunya, Barcelona E 08034

General relativistic multi-group and multi-flavor Boltzmann neutrino transport in spherical symmetry adds a new level of detail to the numerical bridge between microscopic nuclear and weak interaction physics and the macroscopic evolution of the astrophysical object. Although no supernova explosions are obtained, we investigate the neutrino luminosities in various phases of the postbounce evolution for a wide range of progenitor stars between 13 and 40 solar masses. The signal probes the dynamics of material layered in and around the protoneutron star and is, within narrow limits, sensitive to improvements in the weak interaction physics. Only changes that dramatically exceed physical limitations allow experiments with exploding models. We discuss the differences in the neutrino signal and find the electron fraction in the innermost ejecta to exceed 0.5 as a consequence of thermal balance and weak equilibrium at the masscut.

1. Modeling core collapse supernovae on the computer

The traditional scientific experiment may consist of four parts: the preparation of the ingredients, the setup and conduct of a measurement, and a theory to interpret the results. The measurement and equipment present the well defined link between reality and theory. Computer simulations in astrophysics can take a similar rôle. In this case, ingredients are based on theory and the outcome is linked to reality in form of astrophysical observations. For example, supernovae will be reproduced in full detail when all important ingredients are in place. There are, however, lively discussions over which these "important ingredients" are. Self-consistent spherically symmetric simulations try to address a neutrino-driven supernova mechanism [1]. Recently, neutrino transport has been brought close to perfection in the solution of the dynamic Boltzmann transport equation [2] and general relativity has been included with "standard" nuclear and weak interaction physics [3] to form the current state-of-the-art in spherically symmetric simulations, where tightly coupled radiation hydrodynamics is followed in three dimensions: space,

neutrino propagation direction, and neutrino energy. All recent simulations have corroborated the qualitative result that neutrinos don't drive a supernova in spherical symmetry. There is broad agreement that convectional instabilities behind the outwards propagating shock increase the heating efficiency. While multi-dimensional simulations with neutrino transport approximations have delivered encouraging results [4], more recent calculations, combining one-dimensional energy dependent transport with two-dimensional hydrodynamics, again failed to explode the stellar envelope [5]. No doubt that convection is an important ingredient, but there might be more. Convection in the protoneutron star [6], significant rotation, differences between 2D and 3D simulations [7], and magnetic fields [8] are permanent entries on the to do list of future investigations with accurate neutrino transport.

2. Sources and impact of neutrino luminosities

In Fig. (1), we present the luminosities and rms energies in simulations issued from different progenitor stars. From [9] we evolved a 13 $M_\odot$ and a 20 $M_\odot$ star; from [10] we evolved a 15 $M_\odot$, a 25 $M_\odot$, and a 40 $M_\odot$ star; and from [11] a 30 $M_\odot$ star, and a 35 $M_\odot$ star with zero initial metallicity. The simulations with our code AGILE-BOLTZTRAN [12] are based on the Lattimer-Swesty equation of state and "standard" weak interactions [13]. The electron neutrino luminosities are shown in Fig. (1a). The luminosities rise during collapse. Immediately after bounce, a shock is formed at an enclosed mass of 0.53 $M_\odot$. It propagates a density jump outwards that compresses neutrino diffusive material to neutrino opaque matter. This leads to the 4 ms short dip visible in the luminosities right after bounce. As soon as the postshock densities become neutrino transparent, a neutrino burst is released by immediate electron captures on the shock-dissociated nucleons. The evolution up to the neutrino burst is similar in all models because of a self-regulation mechanism during collapse [14]: For larger electron fractions many more protons are available for electron capture and the electron fraction decays more quickly. If electron capture on nuclei were to dominate, this self similarity might not occur. After this initial phase, the neutrino luminosities of the different models open up to individual signatures. The luminosities, as a function of time, reflect the accretion rates (i.e. the density profiles in the outer layers of the progenitor stars) and the gravitational potential at the surface of the protoneutron star [15]. In order to exploit the details of our calculations, we append Fig. (2) for the self-guided contemplation of the interested reader.

The traditional analysis of the neutrino-driven supernova mechanism refers to neutrinospheres, the location where neutrinos have an optical depth of 2/3. Between the neutrino sphere and the shock, neutrino emission and neutrino absorption takes place in the fully dissociated, shock-heated, inwards drifting material. A "gain radius" separates an inner cooling region, where neutrino emission dominates, from an exterior heating region, where neutrino absorption dominates. However, the concept of neutrinospheres is perhaps an oversimplification of the more detailed statistics of neutrino emission as displayed in Fig. (2). Neutrinospheres should not be energy averaged, and the neutrino emission should not be based on a core diffusion scenario alone. Most of the neutrinos are emitted from the base of the cooling region where infalling material settles onto the surface of the protoneutron star. Moreover, the separation into cooling and heating region

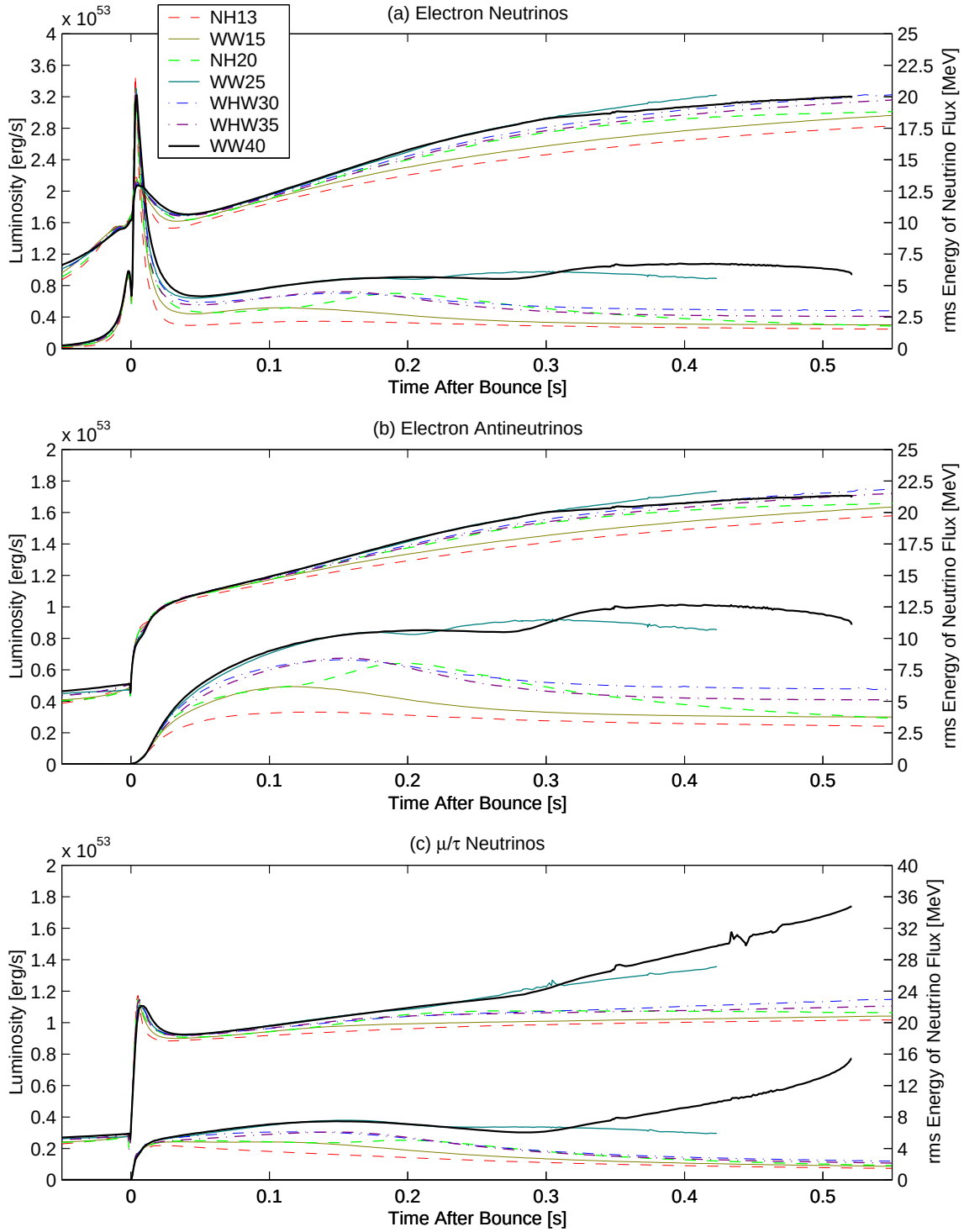

Figure 1. Neutrino luminosities and rms energies of the neutrino flux are shown as a function of time in the evolution of various progenitor models. The upper bundle of curves belongs to the right axis, the lower bundle to the left axis. The quantities are sampled at 500 km in the comoving frame.

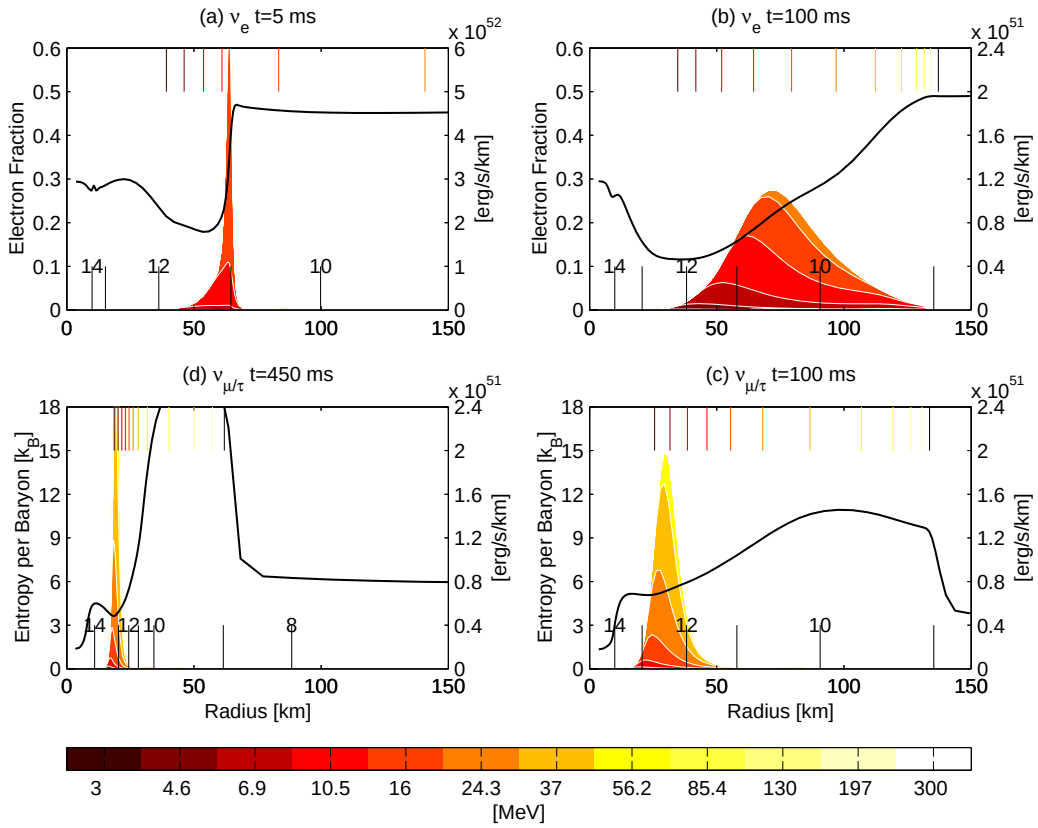

Figure 2. The production site of escaping neutrinos in WW15 is shown as a function of radius in units of [erg/s/km]. The graphs also show profiles of the electron fraction and matter entropy. Markers in the lower part of the graphs indicate the logarithmic density in g/cm^3. In the upper part, they indicate the scattering-dominated neutrinospheres for rising energy groups from left to right according to the legend. Note the sharp profile of the neutrino burst and the broad emission region at 100 ms after bounce. Cooling by μ/τ neutrino emission shrinks at late times to a very narrow radius interval.

refers to the symptom instead of the cause. A separation into regions of thermal balance, weak interaction equilibrium, and non-equilibrium in the spirit of [4] could be more appropriate. The region where matter is in thermal balance and weak equilibrium with the (non-equilibrium!) background neutrino field, is congruent with the former cooling region. Additional energy deposition cannot be achieved by prolonged exposure, only by a change of the matter density or the background neutrino luminosities and rms energies. In Fig. (3a), we compare entropy profiles in the evolution of the 20 $M_\odot$ progenitor to equilibrium values. We note that at 50 ms after bounce infalling matter reaches thermal balance immediately after shock passage. There is no neutrino heating possible. At 100 ms after bounce, the equilibrium entropy is higher than the value reached by shock dissipation. Inflowing material joins the equilibrium line at the former gain radius and a negative entropy gradient becomes manifest. It is, however, counter-intuitive to imagine it as the source of

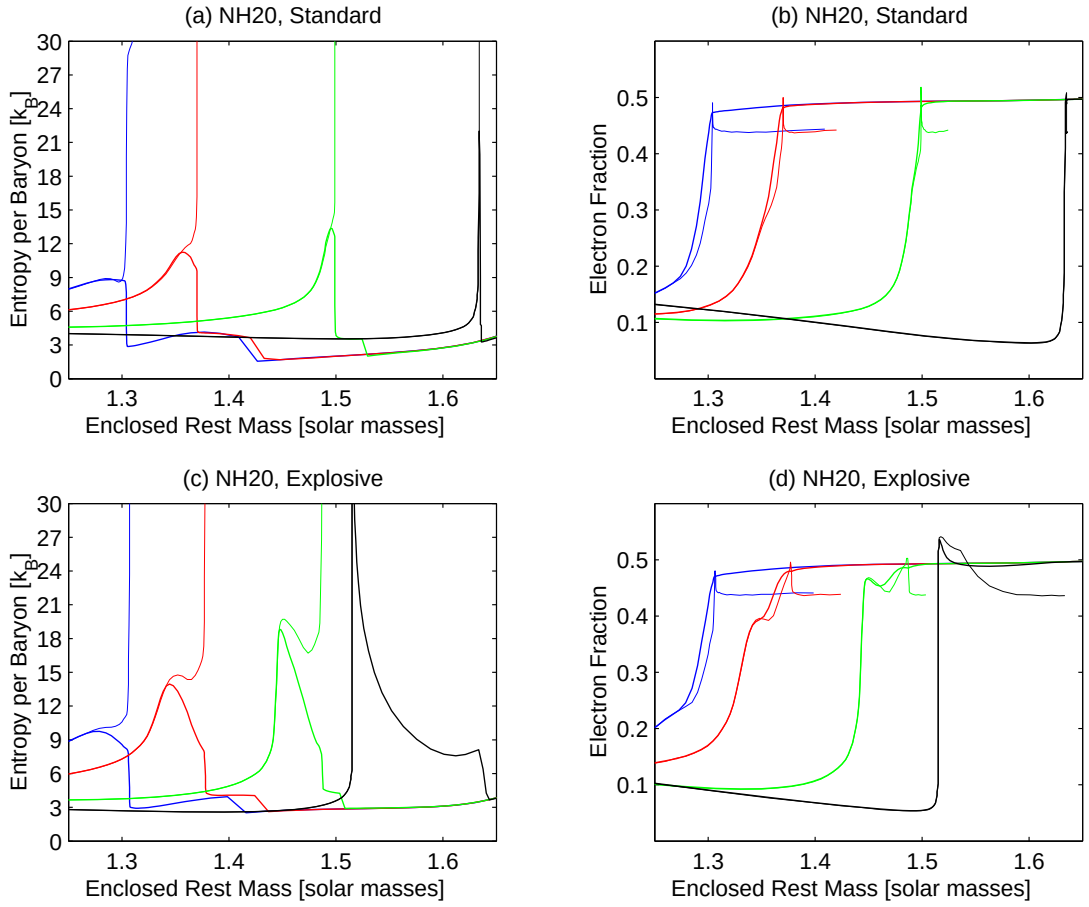

Figure 3. Each graph in this figure shows, from left to right, four snapshots of entropy (a,c) or electron fraction (b,d) profiles as a function of mass at 50, 100, 200, and 450 ms after bounce. The profiles found in the evolution of the full run are represented with a thick line. The thin line shows the asymptotic values, obtained by infinite exposure time to the prevailing neutrino abundances.

the extremely vigorous convection and fast shock expansion found in multi-dimensional simulations of the last decade. After 200 ms, the failure of the model to produce an explosion becomes evident. A similar analysis can be made for the electron fractions shown in graph (b). Infalling matter decreases the electron fraction and increases the entropy. Graphs (a) and (b) also illustrate the possible gain in heating efficiency with convection. Models with stratified hydrodynamics suffer from the fact that the equilibrium entropy is reached in the shells best exposed to neutrino absorption, and that further out, where higher entropies would be allowed, the rates are too low to approach equilibrium during infall time [4]. Convection can mediate in this situation by exchanging material between these two domains such that more material is heated towards equilibrium entropy. It is interesting that the equilibria provide a quantifiable upper and lower bound respectively for entropy and electron fraction changes in the heating region.

3. Sensitivity to nuclear and weak interaction input physics

The failed supernova models in spherical symmetry have, of course, triggered many suggestions to improve the input physics in hopes of overcoming the dead end. One can distinguish improvements that affect the initial bounce-shock energy from improvements that influence the neutrino-driven shock revival. The prompt shock fails in simulations with detailed neutrino transport [16] and loses *all* of its kinetic energy in the neutrino burst long before neutrino heating. Unless there are $\sim 40\%$ changes in the enclosed mass at shock formation, the influence of the bounce-shock energetics to the later shock revival by neutrino heating is marginal. Most interesting for the neutrino-driven mechanism are thus improvements in the standard input physics that alter neutrino luminosities and rms energies. We name some possibilities from inside out: Changes in the high density equation of state would change the compactness of the protoneutron star and with it the position of the accretion layers in the gravitational potential. A more compact protoneutron star would lead to larger infall velocities, higher neutrino luminosities, and higher rms energies in analogy to the impact of general relativistic effects in the core [3]. Moreover, uncertainties are attributed to the neutrino opacities at high densities [17] and corrections for correlations and nucleon recoil should be implemented. However, we speculate that the early luminosities would not dramatically change because the affected density range is enclosed in layers of subnuclear densities, whose still appreciable opacities would prevent dramatic boosts in the neutrino outflow during the first few hundred milliseconds after bounce. Note that the maximum density at 100 ms after bounce is only about twice the saturation density. Additional sources for the μ and τ neutrinos have been suggested: production by bremsstrahlung [18] and production by electron neutrino pair annihilation [19]. Both reactions have been found to locally significantly exceed the importance of the traditional electron-positron pair process. However, changes in self-consistent simulations are small, i.e. on the 10% scale in μ/τ neutrino luminosities [19]. Around the neutrinospheres, a luminosity boost could occur if an equation of state would lead to convective instabilities. However, a stability analysis of the Lattimer-Swesty equation of state in spherical symmetry does not indicate instabilities [6]. Opacity improvements at lower densities are relevant in the early postbounce evolution, because they directly influence the radiation hydrodynamics at and above the surface of the protoneutron star. A list of possible corrections has been presented in [20]. Corrections for weak magnetism and nucleon recoil have been investigated [21] and corrections for the strangeness content of nucleons have been explored [15]. In Fig. (4a), we show the effect of strangeness and weak magnetism on the luminosities and rms energies in a general relativistic evolution of the 15 $M_\odot$ progenitor. Note that, in all three flavors, neutrinos are affected differently than antineutrinos. However, the influence of these corrections on the hydrodynamics are barely visible in our simulation.

4. Phenomenology of neutrino driven explosions in spherical symmetry

The suggested improvements in input physics are quite far from leading to neutrino-driven explosions in the spherically symmetric models. Nevertheless, it is interesting to change input physics beyond physical limits to explore the phenomenology of neutrino-driven explosions with detailed neutrino transport. Explosions can be obtained by the

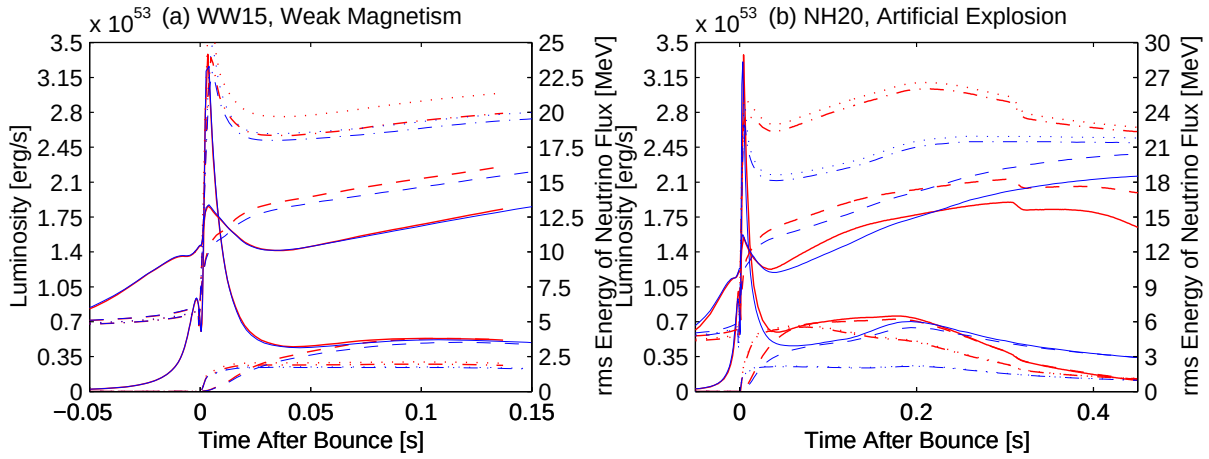

Figure 4. Graph (a) investigates the effect of weak magnetism on electron neutrinos (solid), electron antineutrinos (dashed), μ/τ neutrinos (dash-dotted), and μ/τ antineutrinos (dotted). The improved luminosities and rms energies (thick lines) are compared to standard weak interactions (thin) lines. The same neutrino coding is used in graph (b), where we compare the luminosities and rms energies in an artificial explosion (thick lines) to the standard case (thin lines).

combination of the following measures: (a) The scattering of neutrinos on free nucleons is parameterized to 40% of the full cross section. (b) Only two angles (60, 120 degrees from radius) are considered for the neutrino transport, this increases the heating efficiency and the computing efficiency for parameter studies. (c) The diffusion limit is finite differenced with interpolated transport coefficients (see [12] appendix C for a discussion). The exploding models do still obey lepton number and energy conservation and can be claimed self-consistent in this respect. The luminosities of the artificially exploding model are compared to the luminosities of the standard model in Fig (4b). The heavy neutrinos most effectively reflect the enforced reduction in neutral current reactions. Reduced scattering on the way out reduces the effective path length subject to neutrino electron scattering. The neutrinos cease to thermalize earlier and escape with higher rms energies. Measurements of heavy neutrino properties from supernovae may best single out information about scattering opacities in the protoneutron star. The electron flavor luminosities are about 30% higher than standard during the first 150 ms and drop to 50% lower values later because of the reduced accretion luminosity after the launch of the explosion. Equipartition of the luminosity across the three flavors sets in when the accretion becomes negligible. The equilibrium constraints in Fig. (3c) show that already at 50 ms after bounce the upper entropy bound is much higher than in the standard case, graph (a). As the evolution continues, the neutrino properties are always such that there is ample room for entropy increase. As the explosion proceeds, a large negative entropy gradient develops across a mass of order 0.1 $M_\odot$, in good agreement with analytical estimates [22]. These are future ejecta from the silicon and oxygen layers. All our artificially exploding models produce an electron fraction above 0.5 in the neighborhood of the masscut. As the

material at the mass cut is heated and expanded, the electrons become non-degenerate and the electron chemical potential μ_e falls below the neutron to proton mass difference Q. Rising electron fractions approaching 0.5 have already been predicted in the protoneutron star wind [23]. Here in our high entropy bubble, the tighter bound protons become even more abundant than neutrons as soon as $\mu_e < Q/2$ [24]. Graph (d) demonstrates that material around the masscut actually reaches this weak equilibrium at late times.

Acknowledgements

We acknowledge funding by the NSF under contract AST-9877130, the Oak Ridge National Laboratory, managed by UT-Batelle, LLC, for the U.S. Department of Energy under contract DE-AC05-00OR22725, the Swiss National Science Foundation under contract 20-61822.00, and the DoE HENP SciDAC Program. Our Simulations have been carried out on the NERSC Cray SV-1.

REFERENCES

1. J. R. Wilson, in Numerical Astrophysics, ed. J. M. Centrella, J. M. LeBlanc, and R. L. Bowers, Jones and Bartlett, Boston 1985; H. A. Bethe and J.R. Wilson, ApJ 295 (1985) 14.
2. M. Rampp and H. T. Janka, ApJL 539 (2000) L33; A. Mezzacappa et al., PRL 86 (2001) 1935; T. A. Thompson, A. Burrows, and P. A. Pinto, subm. ApJ, astro-ph/0211194.
3. S. W. Bruenn, K. R. DeNisco, and A. Mezzacappa, ApJ 560 (2001) 326; M. Liebendörfer et al., PRD 63 (2001) 103004.
4. M. Herant et al., ApJ 435 (1994) 339; A. Burrows, J. Hayes, and B. A. Fryxell, ApJ 450 (1995) 830; H.-T. Janka and E. Müller, A&A 306 (1996), 167.
5. A. Mezzacappa et al., ApJ 495 (1998) 911; H.-T. Janka, AAS Meeting 200 (2002) #32.08.
6. J. Wilson and R. Mayle, Phys. Rep. 227 (1993) 97; S. Bruenn and T. Dineva, ApJL 458 (1996) 71.
7. C. F. Fryer and A. Heger, ApJ 541 (2000) 1033; C. F. Fryer and M. S. Warren, ApJL 574 (2002) 65.
8. A. I. MacFadyen and S. E. Woosley, ApJ (1999) 262; C. Thompson, ApJ 534 (2000) 915; J. C. Wheeler et al., ApJ 537 (2000) 810.
9. K. Nomoto and M. Hashimoto, Phys. Rep. 163 (1988) 13.
10. S. E. Woosley and T. A. Weaver, ApJS 101 (1995) 181.
11. S. E. Woosley, A. Heger, and T. A. Weaver, RMP (2002) in press.
12. A. Mezzacappa and O. E. B. Messer, JCAM 109 (1999) 281; M. Liebendörfer, S. K. Rosswog, and F.-K. Thielemann, ApJS 141 (2002) 229; M. Liebendörfer et al., subm. ApJS, astro-ph/0207036.
13. J. Lattimer and F. D. Swesty, Nucl. Phys. A535 (1991) 331; S. W. Bruenn, ApJS 58 (1985) 771.
14. O. E. B. Messer et al., Proc. ESO/MPA/MPE Workshop, ed. B. Leibundgut and W. Hillebrandt, Springer Verlag 2002.
15. M. Liebendörfer et al., Proc. 11th Workshop on Nuclear Astrophysics, ed. W. Hillebrandt and E. Müller, Springer Verlag 2002, astro-ph/0203260.
16. E. S. Myra and S. A. Bludman, ApJ 340 (1989) 384; S. W. Bruenn, ApJ 341 (1989) 385.
17. A. Burrows and R. F. Sawyer, PRC 58 (1998) 554; S. Reddy et al., PRC 59 (1999) 2888.
18. T. A. Thompson, A. Burrows, and J. E. Horvath, PRC 62 (2000) 035802.
19. M. T. Keil, G. G. Raffelt, and H-T. Janka, subm. ApJ, astro-ph/0208035.
20. C. J. Horowitz, PRD 65 (2002) 043001.
21. M. Rampp and H.-T. Janka, Proc. 11th Workshop on Nuclear Astrophysics, ed. W. Hillebrandt and E. Müller, Springer Verlag 2002, astro-ph/0203493.
22. H.-T. Janka, A&A 368 (2001) 527.
23. Y.-Z. Qian and S. E. Woosley, ApJ 471 (1996) 331; T. A. Thompson, A. Burrows, and S. Meyer, ApJ 562 (2001) 887.
24. A. M. Beloborodov, subm. ApJ.